Venture into Water's No Man's Land: Structural Transformations of Solid H_2O under Rapid Compression and Decompression

Chuanlong Lin,[1] Jesse S. Smith,[2] Xuqiang Liu,[1,3] John S. Tse,[1,4,*] and Wenge Yang[1,†]
[1]Center for High Pressure Science and Technology Advanced Research, Shanghai 201203, China
[2]HPCAT, Geophysical Laboratory, Carnegie Institution of Washington, Argonne, Illinois 60439, USA
[3]Key Laboratory for Anisotropy and Texture of Materials, School of Material Science and Engineering, Northeastern University, Shenyang 110819, China
[4]Department of Physics and Engineering Physics, University of Saskatchewan, Saskatoon, S7N 5E2 Canada

(Received 11 June 2018; published 30 November 2018)

Pressure-induced formation of amorphous ices and the low-density amorphous (LDA) to high-density amorphous (HDA) transition have been believed to occur kinetically below a crossover temperature (T_c) above which thermodynamically driven crystalline-crystalline (e.g., ice I_h-to-II) transitions and crystallization of HDA and LDA are dominant. Here we show compression-rate-dependent formation of a high-density noncrystalline (HDN) phase transformed from ice I_c above T_c, bypassing crystalline-crystalline transitions under rapid compression. Rapid decompression above T_c transforms HDN to a low-density noncrystalline (LDN) phase which crystallizes spontaneously into ice I_c, whereas slow decompression of HDN leads to direct crystallization. The results indicate the formation of HDA and the HDN-to-LDN transition above T_c are results of competition between (de)compression rate, energy barrier, and temperature. The crossover temperature is shown to have an exponential relationship with the threshold compression rate. The present results provide important insight into the dynamic property of the phase transitions in addition to the static study.

DOI: 10.1103/PhysRevLett.121.225703

Pressure-induced amorphization of ice I_h and the transformation between low-density amorphous (LDA), high-density amorphous (HDA), and very high-density amorphous (VHDA) ices are of fundamental importance in the study of the physics and chemistry of ice, and have become the prototypical examples in the investigation of amorphization and amorphous-amorphous transitions for many materials [1–6]. The first-order-like LDA-to-HDA transition—extrapolated into so-called water's no man's land where the temperature is between homogeneous nucleation temperature (T_H) [7,8] of supercooled water and crystallization temperature (T_X) [9–12] of amorphous ice—has been hypothesized to terminate at a second critical point (~110 Mbar and ~220 K) [13] and was considered as an indication of a low-density liquid (LDL) to high-density liquid (HDL) transition [14–17]. Both phenomena, pressure-induced amorphization of ice I_h and the LDA-to-HDA transition, were cornerstones of the two-liquid model of water [14–16]. However, studies on the transition mechanism, atomic structures of the noncrystalline phases (namely, LDA, HDA, VHDA, LDL, and HDL), and polyamorphous transition have been hindered by the thermodynamically driven crystalline-crystalline transition and rapid crystallization at higher temperatures [10–12,18–20], leaving a large temperature range (~140–220 K) unexplored.

In the 1990s, a study of emulsified-confined ice I_h indicated a crossover temperature (T_c) at ~160 K at which the phase transition mechanism changes from a thermodynamically driven transition to mechanical instability [17,21], suggested by quasiharmonic lattice-dynamics calculations [22,23]. Recently, *in situ* synchrotron x-ray diffraction measurements on bulk water have shown that the crossover temperature occurs at ~145 K [20]. Ice I_h was found to undergo kinetically controlled amorphization under slow compression (<0.01 GPa/s) of ice I_h up to 1.2 GPa below 145 K. Above 145 K, a thermodynamically driven crystalline-crystalline transition from ice I_h to crystalline ice II (or IX) occurs instead of amorphization. So far, exploration on amorphization of ice I_h and LDA-to-HDA transition is limited up to ~140 K due to rapid crystallization of amorphous ices at higher temperatures [9,20,24], even though LDA and HDA have been studied extensively for the glass-liquid transition and LDL-to-HDL transition below T_X [10–12,18,19,25,26].

Previous studies have shown that it is possible to bypass crystalline-crystalline transitions and form noncrystalline phases by rapid or shock (de)compression [27–30]. For instance, amorphous silicon can be obtained from the high-pressure crystalline phase by rapid (or shock) (de)compression [27,29]. For ice, the phase transitions have been found to be (de)compression-rate dependent. Bauer *et al.* found that ice I_h transformed to ice II under slow compression and to ice III at a moderately higher compression rate (~4 GPa/ min) at 170 K [31]. Chen *et al.* reported a

high-density amorphous ice by rapid compression of liquid water at room temperature [32]. Recently, the high-pressure ice VIII was reported to undergo a metastable melting into a deeply supercooled low-density noncrystalline (LDN) phase under rapid decompression at temperatures of 140–165 K [33]. Motivated by these earlier works, here we examine the possible formation of a high-density noncrystalline (HDN) phase from ice I_c and LDA-to-HDA transition above T_c, bypassing the thermodynamically driven crystalline-crystalline transitions and crystallization of the noncrystalline phases under rapid (de) compression using fast *in situ* x-ray diffraction measurement [29,34]. We show that ice I_c transforms to a high-density noncrystalline phase above T_c under rapid compression. Moreover, under rapid decompression above T_c, the crystallization process can be suppressed and a polyamorphous transition is observed in HDN. Here, the transformed amorphous ice phase above T_c (i.e., within the no man's land) is labeled as HDN to distinguish it from the HDA phase obtained from the pressurization of ice I_h below 145 K [20]. The purpose is to emphasize that the crystalline to amorphous transition can occur in this temperature-pressure region. We do not assert it is a different kind of amorphous state.

The experimental details have been described in previous studies [20,33] and can be found in the Supplemental Material [35]. In the present work, ice I_c was used as the starting material. It was prepared by decompressing high-pressure ice VIII from 4 GPa (or >4 GPa) to ~1 Pa at 180 K, during which the sample ice underwent VIII → VI → II → I*c* transitions. Then the ice I_c phase was cooled from 180 K to a given temperature in preparation for rapid and slow compression. Figures 1(a) and 1(b) show the comparison of experimental results under slow and rapid compression, respectively, at 164 K. Under slow compression at 164 K, ice I_c transforms to ice II at ~0.2 GPa, then to ice VI at ~1.7 GPa, and finally to ice VIII at 3.9 GPa [Fig. 1(a)]. At moderately higher compression rate, ice I_c transforms to the ice IX phase, followed by ice IX → ice VI → ice VIII transitions (Fig. S1 of Supplemental Material [35]). This is consistent with previous reports on the compression-rate-dependent crystalline-crystalline transitions at 170 K [31]. However, under rapid compression (~14.8 GPa/s) from ~1 Pa to 3.5 GPa at 164 K, we found that ice I_c transforms to a noncrystalline phase at ~1.3 GPa with a broad diffraction peak at $Q = 2.27$ Å^{-1}. The diffraction pattern of the noncrystalline phase shows the first broad peak shifted to a higher Q value of 2.40 Å^{-1} at ~2.8 GPa. Then it transforms to ice VIII at ~3.2 GPa under further compression [Fig. 1(b)]. Incidentally, the Q value of the noncrystalline phase is close to that of HDA at 1.3 GPa and VHDA at ~2.8 GPa [20]. The observations indicate a high-density noncrystalline (HDN) phase is formed at 1.3 GPa, which subsequently transforms to a very high-density noncrystalline phase under further

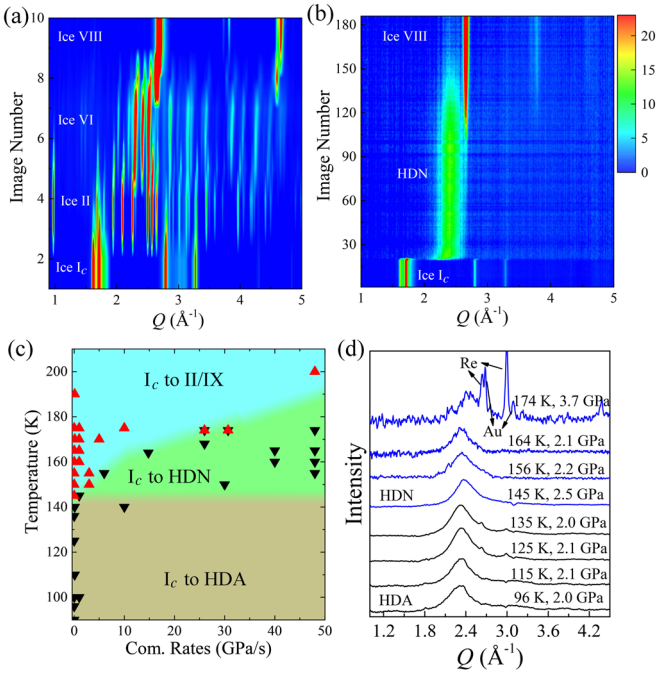

FIG. 1. Compression-rate-dependent formation of the high-density noncrystalline phase. (a) Under slow compression (<0.01 GPa/s) from ~1 Pa to 5 GPa at an interval of ~0.05 GPa with the pressure monitored by an on-line ruby system, the phase transition sequence of ice I_c → ice II → ice VI → ice VIII is observed. The diffraction data is acquired with exposure time of 5 s. (b) Under rapid compression from ~1 Pa to 3.5 GPa with a rate of ~14.8 GPa/s, ice I_c transforms to a noncrystalline phase first, followed by crystallization into ice VIII. During rapid compression, the pressure is increased continuously with the continuous collection of x-ray diffraction images. It should be noted that the rate changes during compression process. The rate of ~14.8 GPa/s is estimated in the pressure range where ice I_c to HDN transition occurs. The exposure time for each diffraction image is 50 ms with images collected at a frequency of 20 Hz. (c) Summary of compression-rate-dependent phase transformation from ice I_c to high-density noncrystalline phase at different temperatures. (d) Comparison of the diffraction patterns of the noncrystalline phases at different temperatures. The high-density noncrystalline phases above 145 K are obtained from ice I_c under rapid compression. The HDA phases below 145 K are obtained by static compression of ice I_h [20].

compression. This is similar to the occurrence of HDA and VHDA ices. Compared with the gradual crystallization of the very HDN phase, the formation of HDN is abrupt within a narrow pressure range [Fig. 1(b), and see integrated diffraction patterns in Fig. S2 of Supplemental Material [35]]. It should be noted that the starting sample used here is ice I_c. Structurally it is slightly different from ice I_h, and the amorphization pressure is 0.05 GPa lower than ice I_h [40]. The present work does not suggest that ice I_h has the same compression-rate-dependent amorphization above T_c, although the difference is expected to be small.

In order to probe the effects of temperature and compression rate on the phase transitions, we have conducted systematic investigations at different temperatures and compression rates. Figure 1(c) summarizes the experimental results. It shows that the formation of HDN from ice I_c under rapid compression is also observed at a temperature range between 145 and 174 K [Fig. 1(c) and Figs. S3–S7 of Supplemental Material [35]], all above the previously reported crossover temperature ($T_c \sim 145$ K) [20]. At these temperatures and a moderate compression rate, however, ice I_c transforms to ice II or IX [Fig. 1(c)], followed by transformations to ice VI and VIII [20]. Above 145 K, the phase transformation of ice I_c is compression-rate dependent. This is in contrast to the compression-rate-independent amorphization below 145 K. At a given temperature (T), it appears that there exists a threshold compression rate required for the formation of the HDN phase. Below 160 K, the minimum compression rate gradually increases as temperature increases. At $T > 160$ K, the compression rate required for producing the HDN phase increases rapidly with increasing temperature. Figure 1(d) shows the integrated diffraction patterns of HDN at different temperatures with background subtracted, compared with those of HDA transformed from ice I_h below 145 K. It is clearly seen that the diffraction patterns of the HDN phase are similar to those of HDA. From x-ray diffraction patterns, we cannot distinguish whether HDN is a solid amorphous ice or a viscous HDL as suggested previously [18,26,41–43], even though HDN is observed above the glass transition temperature of HDA.

The HDN sample at a given pressure is heated to monitor the stability and crystallization behavior. In the experiments, the HDN phase is obtained by rapid compression of ice I_c up to ~2.0 GPa at 150 K, and then the pressure is adjusted to the targeted value using double membrane pressure control [34]. Depending on the pressure, crystallization of the noncrystalline phase into different dense crystalline ices is observed (Fig. 2). It is found that the noncrystalline phase transforms to ice XII at ~1.2 GPa during heating from 169 to 177 K [Fig. 2(a)] and to ice VI at 2.1 GPa from 170 to 176 K [Fig. 2(b)]. The crystallization into different crystalline ices indicates that the noncrystalline phases at ~1.2 GPa and ~2.1 GPa may have different local structures, corresponding to HDA and VHDA. These observations are consistent with previous reports on *ex situ* x-ray diffraction measurements [44]. Instead of the initial homogeneous powder patterns, the diffraction patterns of ice XII and VI consist of sharp diffraction spots, indicating single crystals or polycrystalline grains of ice XII [Fig. 2(c)] and VI [Fig. 2(d)]. The results indicate grain coalescence during the crystallization process of the HDN phase. In contrast, there is no grain growth or grain coalescence in the crystalline-crystalline transitions (ice ice $I_c \rightarrow$ ice II $\rightarrow$ ice VI $\rightarrow$ ice VIII) during compression.

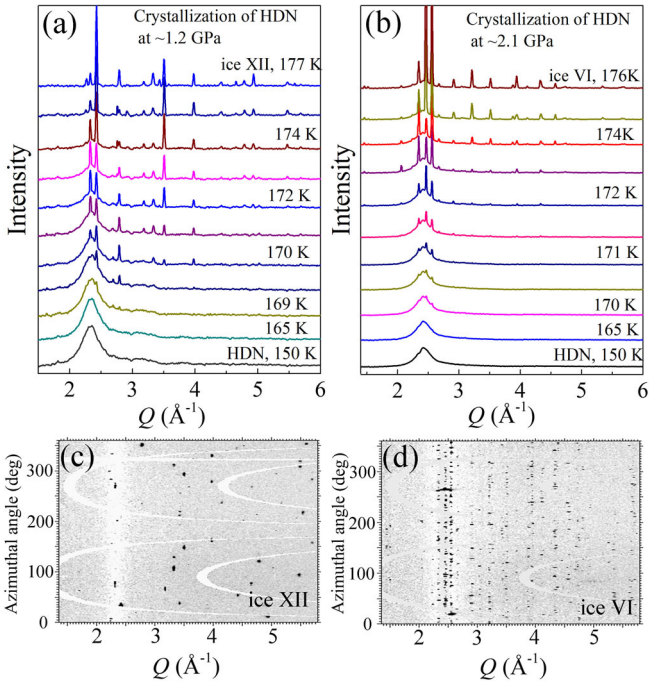

FIG. 2. Crystallization of high-density noncrystalline phase at 1.2 and 2.1 GPa by warming. (a) HDN is heated from 150 to 177 K. It starts to crystallize into ice XII at ~169 K, and completes at ~177 K. (b) HDN is heated from 150 K. It crystallizes into ice VI at ~170 K and is complete at ~176 K. (c),(d) Azimuthally unwrapped x-ray diffraction images of ice XII and VI crystallized from HDN at ~1.2 and ~2.1 GPa, respectively. The diffraction images, subtracted by an image of the noncrystalline phase as background, are obtained by caking (unrolling) the two-dimensional x-ray diffraction images. The horizontal axis is Q value. The vertical axis is azimuth angle. The white broad band at ~2.3 $Å^{-1}$ indicates the first sharp peak of HDN. The black dots are the diffraction peaks from crystalline phases of ice XII and VI. The half ellipses are the masks from the area detector.

Figure 3 shows the phase transitions of HDN under decompression at different ramp rates. In the experiments, HDN is obtained by rapid compression of ice I_c at 158 K. After observing the HDN phase, the pressure is released immediately at different decompression rates. We find that the phase transition of HDN under decompression is dependent on the ramp rates. At a slow decompression rate (<0.01 GPa/s), HDN phase crystallizes into ice VI and transforms to ice II and eventually to I_c [Fig. 3(a)]. At a high decompression rate (~10 GPa/s), instead of direct crystallization, the HDN phase is found to transform to a low-density noncrystalline phase at ~1 Pa [Fig. 3(b)]. The LDN subsequently crystallizes into ice I_c. Previous results show that the LDN phase could be a deeply supercooled low-density liquid phase [33], indicated by the temperature-dependent crystallization behavior.

Figure 4 summarizes the compression-rate-dependent formation of high-density noncrystalline phases at various

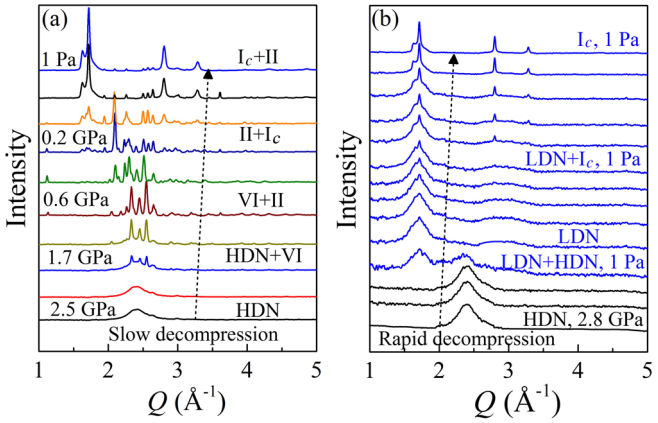

FIG. 3. Rate-dependent phase transformation of HDN at 158 K under decompression. (a) Slow decompression of HDN leads to crystallization into ice VI, followed by ice VI → ice II → ice I_c transitions. (b) Rapid decompression (~10 GPa/s) of HDN results in the direct transformation to a low-density noncrystalline phase.

temperatures, compared to the formation of low-density noncrystalline (LDA and LDL) phases. With increasing temperature, the minimum compression or decompression rate required for the formation of noncrystalline phases increases (Fig. 4). The threshold (de)compression rate has a steep initial increase at low temperature and slight increase at higher temperature. It should be noted that the temperature at the threshold compression rate corresponds to a crossover temperature, namely, above which thermodynamically driven crystalline-crystalline transitions (i.e., ice I_c-to-II for compression and VIII-to-VI for decompression) are observed and below which the noncrystalline phases form. Noticeably, the transition temperature changes with compression rate. Therefore, how is the threshold compression rate related to the transition temperature (T_c)?

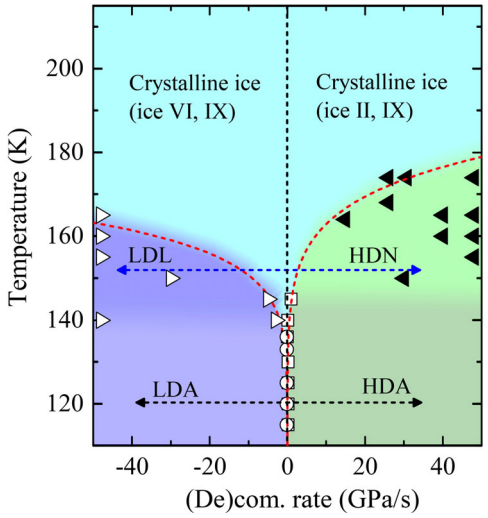

FIG. 4. (De)compression-rate-dependent (negative decompression, positive compression) formation of noncrystalline phases at different temperatures. Black solid triangles represent high-density noncrystalline phase obtained by rapid compression in present work. Open squares and circles indicate the high-density amorphous and low-density phases previously obtained by static compression or decompression [20]. Open triangles are low-density noncrystalline phase formed from high-pressure ice VIII under rapid decompression [33]. Red dashed line is the fitting line.

In order to bypass thermodynamically driven I_c-to-II (or ice IX) transition at a given temperature, the compression time (Δt) required for passing the equilibrium stable pressure range (ΔP) of ice II should be shorter than the characteristic transition time (τ) of ice I_c-to-II transition. The transition time (τ) is determined by the Arrhenius equation [45–48], namely, the rate constant ($1/\tau$) which is proportional to $\exp(-\Delta E/k_B T)$, where ΔE is the energy barrier for the phase transition and k_B is the Boltzmann constant. The thermal energy ($k_B T$) governs the probability of the water to overcome the energy barrier. The compression time in bypassing the pressure region of ice II is determined by $\Delta t = \Delta P/\beta$, where β is the compression rate. The HDN phase is formed when $\Delta t < \tau$, namely, ice I_c bypasses the equilibrium pressure region of ice II on a shorter timescale so that the ice I_c-to-II transition does not have enough time to occur. For simplicity, let us assume ΔE and ΔP are independent of pressure and temperature, and the threshold compression rate (β_c) is determined by $\Delta t = \tau$. Then we can obtain $\beta_c = C_0 \exp(-\Delta E/k_B T_c)$, where C_0 is a constant with units of GPa/s. It is clear that the formation of the HDN phase is the result of competition among the external compression rate, temperature, and energy barrier. It is more complicated in reality as both ΔE and ΔP also change with pressure and temperature.

The red dashed lines in Fig. 4 are fits of the experimental compression and decompression results to the Arrhenius law. Reasonable agreements are obtained with ΔE of 24(2) kJ/mol and C_0 of 6.4×10^8 GPa/s for compression and ΔE of 26(2) kJ/mol and C_0 of 1.3×10^{10} GPa/s for decompression. It should be noted that ΔE represents an average order of magnitude estimated as the value is expected to vary with pressure during (de)compression [48]. The characteristic time of the ice I_c-to-II transition as a function of temperature can be estimated based on the fitting results. For example, τ is estimated to be $\sim 10^7$ s for the formation of HDA at liquid nitrogen temperature, which is much longer than the experimental timescale (minutes or hours). This explains previous observations that ice I_h can bypass the pressure region of ice II and transforms to a metastable amorphous phase under compression to 1.2 GPa [20]. The previously reported HDA phase can be viewed as the case of slow compression (open squares in Fig. 4). With increasing temperature, τ decreases exponentially from $\sim 10^7$ s at 77 K to $\sim 10^{-2}$ s at 174 K. Therefore, at high temperature, the characteristic time of the phase transition from 145 to 174 K is comparable to the experimental timescale. This interpretation is consistent with the

observed compression-rate-dependent phase transition pathway. Extrapolation of the present results to higher temperature towards the proposed second critical point (110 MPa, 220 K) [13] suggests the timescale is in the nano- to microsecond regime. The formation of HDN may still be possible but will require ultrafast *in situ* measurement at a very high compression rate.

The mechanism of the decompression-induced HDA-to-LDA transition is also determined by the competition between the energy barrier for crystallization of the non-crystalline phases, temperature, and decompression rate. Suppression of crystallization of HDN is observed in rapid decompression as the transformation from HDN to LDL can be observed above 140 K (blue arrow in Fig. 4). The present results expand the temperature range from the previous report on HDA-to-LDA transition (black arrow in Fig. 4). The well-known HDA-to-LDA transition below 140 K can be viewed as a case of slow decompression, analogous to the pressure-induced amorphization. At a given temperature, the threshold decompression rate for the formation of LDL from ice VIII [33] is larger than the minimum compression rate for formation of HDN from ice I_c. From the boundary between crystalline ice and non-crystalline phases shown in Fig. 4, the temperature range for the formation of LDL is apparently smaller than that of HDN, and there may be a critical temperature above which the transformation between HDN and LDL will not occur even with very rapid decompression.

The experimental evidence provided here clearly shows the importance of the role of kinetics in the structural phase transitions between crystalline and amorphous ices in no man's land. The results show that the suggestion of the existence of a critical temperature T_c, the crossover temperature between homogeneous nucleation and amorphization, is not founded on firm thermodynamic grounds. It is also shown that this "imaginary" phase boundary can be traversed by rapid compression (i.e., control of the kinetics). The compression of ice I_h to HDA at low temperature is due to insufficient external energy to overcome the energy barrier required to rearrange the hydrogen bonds to the thermodynamically stable crystalline structure, possibly ice VI (or XV). We speculate that a crystalline-crystalline transition for ice I_h could eventually be achieved at low temperatures (<100 K) if compressed in a hydrostatic medium at a very slow rate allowing the relaxation of the frustrated intermediate amorphous structure. Moreover, the experimental decompression results show that the HDN → LDN phase boundary does not extrapolate to the proposed second critical point.

The authors thank Curtis Kenney-Benson and Richard Ferry for technical support and would like to thank the Science Challenge Project (TZ2016001) and National Nature Science Foundation of China (U1530402) for financial support. HPCAT operations are supported by DOE−NNSA under Award No. DE-NA0001974, with partial instrumentation funding by NSF. APS is supported by DOE−BES, under Contract No. DE-AC02-06CH11357 by UChicago Argonne, LLC.

*Corresponding author.
john.tse@usask.ca
†Corresponding author.
yangwg@hpstar.ac.cn

[1] O. Mishima, L. D. Calvert, and E. Whalley, Nature (London) **310**, 393 (1984).
[2] O. Mishima, L. D. Calvert, and E. Whalley, Nature (London) **314**, 76 (1985).
[3] R. J. Hemley, A. P. Jephcoat, H. K. Mao, L. C. Ming, and M. H. Manghnani, Nature (London) **334**, 52 (1988).
[4] J. P. Itie, A. Polian, G. Calas, J. Petiau, A. Fontaine, and H. Tolentino, Phys. Rev. Lett. **63**, 398 (1989).
[5] M. B. Kruger and R. Jeanloz, Science **249**, 647 (1990).
[6] L. Thomas and G. Nicolas, J. Phys. Condens. Matter **18**, R919 (2006).
[7] B. J. Mason, Adv. Phys. **7**, 221 (1958).
[8] J. A. Sellberg *et al.*, Nature (London) **510**, 381 (2014).
[9] O. Mishima, J. Chem. Phys. **100**, 5910 (1994).
[10] G. P. Johari, A. Hallbrucker, and E. Mayer, Nature (London) **330**, 552 (1987).
[11] R. S. Smithand B. D. Kay, Nature (London) **398**, 788 (1999).
[12] O. Andersson, Proc. Natl. Acad. Sci. U.S.A. **108**, 11013 (2011).
[13] O. Mishima and H. E. Stanley, Nature (London) **392**, 164 (1998).
[14] P. H. Poole, F. Sciortino, U. Essmann, and H. E. Stanley, Nature (London) **360**, 324 (1992).
[15] K. Amann-Winkel, R. Bohmer, F. Fujara, C. Gainaru, B. Geil, and T. Loerting, Rev. Mod. Phys. **88**, 011002 (2016).
[16] P. Gallo, K. Arnann-Winkel, C. A. Angell, M. A. Anisimov, F. Caupin, C. Chakravarty, E. Lascaris, T. Loerting, A. Z. Panagiotopoulos, J. Russo, J. A. Sellberg, H. E. Stanley, H. Tanaka, C. Vega, L. M. Xu, and L. G. M. Pettersson, Chem. Rev. **116**, 7463 (2016).
[17] O. Mishima and H. E. Stanley, Nature (London) **396**, 329 (1998).
[18] C. R. Hill, C. Mitterdorfer, T. G. A. Youngs, D. T. Bowron, H. J. Fraser, and T. Loerting, Phys. Rev. Lett. **116**, 215501 (2016).
[19] F. Perakis, K. Amann-Winkel, F. Lehmkühler, M. Sprung, D. Mariedahl, J. A. Sellberg, H. Pathak, A. Späh, F. Cavalca, D. Schlesinger, A. Ricci, A. Jain, B. Massani, F. Aubree, C. J. Benmore, T. Loerting, G. Grübel, L. G. M. Pettersson, and A. Nilsson, Proc. Natl. Acad. Sci. U.S.A. **114**, 8193 (2017).
[20] C. L. Lin, X. Yong, J. S. Tse, J. S. Smith, S. V. Sinogeikin, C. Kenney-Benson, and G. Y. Shen, Phys. Rev. Lett. **119**, 135701 (2017).
[21] O. Mishima, Nature (London) **384**, 546 (1996).
[22] J. S. Tse, D. D. Klug, C. A. Tulk, I. Swainson, E. C. Svensson, C. K. Loong, V. Shpakov, V. R. Belosludov, R. V. Belosludov, and Y. Kawazoe, Nature (London) **400**, 647 (1999).

[23] J. S. Tse, J. Chem. Phys. **96**, 5482 (1992).
[24] E. L. Gromnitskaya, O. V. Stal'gorova, V. V. Brazhkin, and A. G. Lyapin, Phys. Rev. B **64**, 094205 (2001).
[25] M. S. Elsaesser, K. Winkel, E. Mayer, and T. Loerting, Phys. Chem. Chem. Phys. **12**, 708 (2010).
[26] K. Amann-Winkel, C. Gainaru, P. H. Handle, M. Seidl, H. Nelson, R. Böhmer, and T. Loerting, Proc. Natl. Acad. Sci. U.S.A. **110**, 17720 (2013).
[27] M. Gamero-Castano, A. Torrents, L. Valdevit, and J. G. Zheng, Phys. Rev. Lett. **105**, 145701 (2010).
[28] S. T. Zhao, B. Kad, C. E. Wehrenberg, B. A. Remington, E. N. Hahn, K. L. More, and M. A. Meyers, Proc. Natl. Acad. Sci. U.S.A. **114**, 9791 (2017).
[29] J. S. Smith, S. V. Sinogeikin, C. L. Lin, E. Rod, L. G. Bai, and G. Y. Shen, Rev. Sci. Instrum. **86**, 072208 (2015).
[30] D. R. Clarke, M. C. Kroll, P. D. Kirchner, R. F. Cook, and B. J. Hockey, Phys. Rev. Lett. **60**, 2156 (1988).
[31] M. Bauer, M. S. Elsaesser, K. Winkel, E. Mayer, and T. Loerting, Phys. Rev. B **77**, 220105 (2008).
[32] J. Y. Chen and C. S. Yoo, Proc. Natl. Acad. Sci. U.S.A. **108**, 7685 (2011).
[33] C. Lin, S. S. Smith, S. V. Sinogeikin, and G. Shen, Proc. Natl. Acad. Sci. U.S.A. **115**, 2010 (2018).
[34] S. V. Sinogeikin, J. S. Smith, E. Rod, C. L. Lin, C. Kenney-Benson, and G. Y. Shen, Rev. Sci. Instrum. **86**, 072209 (2015).
[35] See Supplemental Material at http://link.aps.org/supplemental/10.1103/PhysRevLett.121.225703 for experimental details and additional x-ray diffraction results at various temperatures, which includes Refs. [36–39].
[36] R. Hrubiak, S. Sinogeikin, E. Rod, and G. Y. Shen, Rev. Sci. Instrum. **86**, 072202 (2015).
[37] H. K. Mao, J. Xu, and P. M. Bell, J. Geophys. Res. **91**, 4673 (1986).
[38] J. Yen and M. Nicol, J. Appl. Phys. **72**, 5535 (1992).
[39] C. Prescher and V. B. Prakapenka, High Press. Res. **35**, 223 (2015).
[40] M. A. Floriano, Y. P. Handa, D. D. Klug, and E. Whalley, J. Chem. Phys. **91**, 7187 (1989).
[41] T. Loerting, V. Fuentes-Landete, P. H. Handle, M. Seidl, K. Amann-Winkel, C. Gainaru, and R. Bohmer, J. Non-Cryst. Solids **407**, 423 (2015).
[42] P. H. Handle, M. Seidl, and T. Loerting, Phys. Rev. Lett. **108**, 225901 (2012).
[43] M. Seidl, M. S. Elsaesser, K. Winkel, G. Zifferer, E. Mayer, and T. Loerting, Phys. Rev. B **83**, 100201 (2011).
[44] S. Klotz, G. Hamel, J. S. Loveday, R. J. Nelmes, and M. Guthrie, Z. Kristallogr. **218**, 117 (2003).
[45] N. V. C. Shekar and K. G. Rajan, Bull. Mater. Sci. **24**, 1 (2001).
[46] A. K. Singh, Mater. Sci. Forum **3**, 291 (1985).
[47] S. Glasstone, K. J. Laidler, and H. Eyring, *The Theory of Rate Processes* (McGraw-Hill, New York, 1941).
[48] C. L. Lin, J. S. Smith, S. V. Sinogeikin, C. Park, Y. Kono, C. Kenney-Benson, E. Rod, and G. Y. Shen, J. Appl. Phys. **119**, 045902 (2016).